Pergamon

Cement and Concrete Research 30 (2000) 1267–1276

CEMENT AND CONCRETE RESEARCH

The effect of compressive stress on thermal and hygric properties of Portland cement mortar in wide temperature and moisture ranges

R. Černý[a,*], J. Maděra[a], J. Poděbradská[a], J. Toman[b], J. Drchalová[b], T. Klečka[c], K. Jurek[d], P. Rovnaníková[e]

[a]*Department of Structural Mechanics, Faculty of Civil Engineering, Czech Technical University, Thákurova 7, 166 29 Prague 6, Czech Republic*
[b]*Department of Physics, Faculty of Civil Engineering, Czech Technical University, Thákurova 7, 16629 Prague 6, Czech Republic*
[c]*Klokner Institute, Czech Technical University, Šolínova 7, 160 00 Prague 6, Czech Republic*
[d]*Institute of Physics, The Academy of Sciences of the Czech Republic, Na Slovance 2, 180 40 Prague 8, Czech Republic*
[e]*Institute of Chemistry, Faculty of Civil Engineering, Technical University of Brno, Žižkova 17, 662 37 Brno, Czech Republic*

Received 23 August 1999; accepted 24 May 2000

Abstract

Basic thermal and hygric parameters of cement mortar — namely, the thermal conductivity, the linear thermal and hygric expansion coefficients, moisture diffusivity, and water vapor permeability — are determined in dependence on the applied mechanical load inducing compressive stress in the samples ranging from 0% to 90% of compressive strength. The measurements are performed in wide temperature and moisture ranges, from 20°C to 1000°C and from the dry state to the saturation water content. The measured results show that both thermal and hygric parameters of cement mortar are affected only by compressive stress of 90% of the compressive strength of the material and higher, in a significant way. Scanning electron microscope images and porosimetric measurements reveal that the most probable reason for the observed differences in thermal and hygric parameters is the appearance of cracks with a typical width of 1–2 μm.

Keywords: Transport properties; Expansion; Hygric properties; SEM; Mercury porosimetry

1. Introduction

Thermal and hygric properties of concretes, cement mortars, and cement pastes are measured at room temperature in standard conditions, in most cases. For many applications of concrete in building structures, is it quite sufficient as usual environmental exposure is within the range from about −20°C to +50°C. However, some concrete structures can be exposed to elevated or high temperatures during their lifetime. Fire resistance problems of concrete structures can be considered probably as the most important example in this respect, but special industrial applications of concrete, such as in blast furnaces, nuclear safety-related structures or heat pipes also become of great significance. In such conditions, high temperature values of thermal parameters have to be determined in order to analyze the behavior of the particular structures already in the design phase in a proper way.

We will introduce several examples of measurements of thermal parameters in high temperature range determined by various investigators. Thermal expansion of cement paste in the temperature range to 800°C was measured by Philleo [1] and Harada et al. [2], thermal expansion of various concretes up to 1000°C for instance by Schneider [3] or Komarovskii [4]. Specific heat of cement paste was determined by Harmathy [5], specific heat of various types of concrete by Harmathy and Allen [6], Hildenbrand et al. [7]. Thermal conductivity of cement paste was measured by Harmathy [5], thermal conductivity of concrete by Schneider [3], Harmathy and Allen [6], Hildenbrand et al. [7]. A more comprehensive survey of the thermal properties of concrete at high temperatures measured until ∼1992 can be found by the reader in the book by Bažant and Kaplan [8].

Hygric parameters of cement pastes and concretes were measured at normal conditions very frequently. For instance,

* Corresponding author. Tel.: +42-2-24-35-44-29; fax: +42-2-24-31-07-75.
E-mail address: cernyr@fsv.cvut.cz (R. Černý).

0008-8846/00/$ – see front matter
PII: S0008-8846(00)00310-0

moisture diffusivity of concrete was measured by Bažant and Najjar [9], water permeability of cement paste by Powers and Brownyard [10], water permeability of concrete by El-Dieb and Hooton [11], Halamickova et al. [12], etc. On the other hand, there are very few measurements of hygric parameters in non-standard conditions; for instance, Bažant and Thonguthai [13] studied moisture diffusivity for temperatures above 100°C.

Concrete structures are practically always exposed to mechanical load producing compressive or tensile stress in the material. However, the effect of mechanical load on thermal and hygric properties was investigated very seldom, until now. We can mention the work by Bažant et al. [14], where the influence of crack on drying permeability of concrete in room temperature conditions was studied, as one of very few examples.

In this paper, we study the main thermal and hygric properties of Portland cement mortar, namely, the thermal conductivity, the linear thermal expansion coefficient, the moisture diffusivity, the water vapor permeability, and the linear hygric expansion coefficient in dependence on compressive stress up to 90% of compressive strength, which was imposed on material samples prior to the measurements. Thermal conductivity is determined for a dry material in the temperature range to 800°C, and for a moist material with moisture content ranging from dry stage to maximum water saturation in the room temperature conditions. The linear thermal expansion coefficient is measured for a dry material up to 1000°C. The hygric transport parameters are measured for characteristic values of the moisture content in room temperature conditions, with the linear hygric expansion coefficient at room temperature in a wide moisture range up to maximum water saturation.

2. Methods for measuring the thermal and hygric parameters

2.1. Thermal conductivity

In measuring the thermal conductivity in room temperature conditions, we employed a commercial device Shotherm QTM (Showa Denko) which is based on the hot wire principle.

For the determination of thermal conductivity in the high-temperature region, we used a double integration method we developed earlier (see Ref. [15]) which is based on the solution of an inverse problem of heat conduction. We will introduce shortly the basic principles of the derivation of the method for the convenience of the reader.

We have the one-dimensional heat conduction equation in the form:

$$\rho c\frac{\partial T}{\partial t}=\frac{\partial}{\partial x}\left(K\frac{\partial T}{\partial x}\right), \tag{1}$$

where K is the thermal conductivity, ρ the density, and c the specific heat.

We suppose $T(t)$ and $T(x)$ to be monotonous functions and choose a constant value of temperature, $\tau=T(x,t)$. Then there must exist one-to-one parameterizations $x=x_0(\tau,t)$, $t=t_0(\tau,x)$ where both x_0 and t_0 are monotonous functions. Considering this fact, an integration of heat conduction [Eq. (1)] by x and t leads to:

$$\int_{t_1}^{t_2}\int_0^{x_0(\tau,t)}\rho c\frac{\partial T}{\partial t}(x,t)\mathrm{d}x\mathrm{d}t=K(\tau)\int_{t_1}^{t_2}\frac{\partial T}{\partial x}(x_0(\tau,t),t)\mathrm{d}t+\int_{t_1}^{t_2}j_{\mathrm{q}}(0,t)\mathrm{d}t, \tag{2}$$

where the heat flux at $x=0$, $j_{\mathrm{q}}(0,t)$, reads [Eq. (3)]:

$$j_{\mathrm{q}}(0,t)=-K(T)\frac{\partial T}{\partial x}(0,t). \tag{3}$$

The left-hand side of the Eq. (2) can be modified by accounting for the shape of the integration area [Eq. (4)]:

$$\begin{aligned}\mathrm{LS}&=\int_{t_1}^{t_2}\int_0^{x_0(\tau,t)}\rho c\frac{\partial T}{\partial t}(x,t)\mathrm{d}x\mathrm{d}t\\&=\int_0^{x_0(\tau,t_1)}\int_{t_1}^{t_2}\rho c\frac{\partial T}{\partial t}(x,t)\mathrm{d}x\mathrm{d}t+\int_{x_0(\tau,t_1)}^{x_0(\tau,t_2)}\int_{t_0(\tau,x)}^{t_2}\rho c\frac{\partial T}{\partial t}(x,t)\mathrm{d}x\mathrm{d}t.\end{aligned} \tag{4}$$

Denoting $I_{\mathrm{T}}=\int\rho c(\partial T/\partial t)\mathrm{d}t=\int\rho(T)c(T)\mathrm{d}T$, we obtain:

$$\begin{aligned}\mathrm{LS}&=\int_0^{x_0(\tau,t_1)}(I_{\mathrm{T}}(T(x,t_2))-I_{\mathrm{T}}(T(x,t_1)))\mathrm{d}x+\int_{x_0(\tau,t_1)}^{x_0(\tau,t_2)}(I_{\mathrm{T}}(T(x,t_2))-I_{\mathrm{T}}(\tau))\mathrm{d}x\\&=\int_0^{x_0(\tau,t_2)}I_{\mathrm{T}}(T(x,t_2))\mathrm{d}x-\int_0^{x_0(\tau,t_1)}I_{\mathrm{T}}(T(x,t_1))\mathrm{d}x-I_{\mathrm{T}}(\tau)[x_0(\tau,t_2)-x_0(\tau,t_1))].\end{aligned} \tag{5}$$

Substituting Eq. (5) into Eq. (2), we get:

$$\begin{aligned}K(\tau)=\frac{1}{\int_{t_1}^{t_2}\frac{\partial T}{\partial x}(x_0(\tau,t),t)\mathrm{d}t}\Bigg(&\int_0^{x_0(\tau,t_2)}I_{\mathrm{T}}(T(x,t_2))\mathrm{d}x-\int_0^{x_0(\tau,t_1)}I_{\mathrm{T}}(T(x,t_1))\mathrm{d}x\\&-I_{\mathrm{T}}(\tau)[x_0(\tau,t_2)-x_0(\tau,t_1)]-\int_{t_1}^{t_2}j_{\mathrm{q}}(0,t)\mathrm{d}t\Bigg).\end{aligned} \tag{6}$$

In Eq. (6), some difficulties may arise with the determination of the heat flux $j_{\mathrm{q}}(0,t)$. Basically, we have two possibilities how to deal with this problem: either to measure $j_{\mathrm{q}}(0,t)$ directly or to calculate it from the known temperature field $T(x,t)$. In the high temperature range we are interested in, measuring $j_{\mathrm{q}}(0,t)$ is relatively difficult. Therefore, we choose the numerical

treatment, and supposing that in the initial state the boundary condition for temperature on the opposite side of the one-sided heated sample is not yet influencing the temperature field, we calculate $j_q(0,t)$ from the formula [Eq. (7)]:

$$j_q(0,t) = \frac{1}{t_2 - t_1} \int_0^l [\rho(T)c(T)T(x,t_2) - \rho(T)c(T)T(x,t_1)]\mathrm{d}x, \quad (7)$$

where l is the length of the one-dimensional sample.

As follows from Eq. (6), in determining thermal conductivity, we need the dependences of specific heat and density on temperature. The specific heat in the temperature range to 1000°C was measured using our non-adiabatic method (see Ref. [16]); density temperature dependence was determined by thermogravimetry.

2.2. The linear thermal and hygric expansion coefficients

The infinitesimal change of length due to the change of temperature is defined by [Eq. (8)]:

$$\mathrm{d}l_T = l_0 \alpha_T \mathrm{d}T, \quad (8)$$

where l_0 is the length at the reference temperature T_0, α_T is the linear thermal expansion coefficient. In an analogous way, the linear hygric expansion coefficient α_u can be defined [Eq. (9)]:

$$\mathrm{d}l_u = l_0 \alpha_u \mathrm{d}u, \quad (9)$$

where [Eq. (10)]:

$$u = 100 \frac{m_m - m_d}{m_d} \quad (10)$$

is the moisture content in mass percent, m_m is the mass of the moistened material, m_d the mass of the dried material.

Applying, in the first approximation, the superposition principle to the length changes due to temperature and moisture, we arrive at [Eq. (11)]:

$$\mathrm{d}l = \mathrm{d}l_T + \mathrm{d}l_u = l_0(\alpha_T \mathrm{d}T + \alpha_u \mathrm{d}u). \quad (11)$$

Defining the normal strain ϵ as [Eq. (12)]:

$$\epsilon = \frac{\Delta l}{l} = \frac{1}{l_0} \int_{l_1}^{l_2} \mathrm{d}l, \quad (12)$$

we obtain:

$$\epsilon(u,T) = \epsilon_T(u_0,T) + \epsilon_u(u,T_0) = \int_{T_0}^{T} \left(\frac{\partial \epsilon}{\partial T}\right)_u \mathrm{d}T + \int_{u_0}^{u} \left(\frac{\partial \epsilon}{\partial u}\right)_T \mathrm{d}u = \int_{T_0}^{T} \alpha_T \mathrm{d}T + \int_{u_0}^{u} \alpha_u \mathrm{d}u. \quad (13)$$

Measuring the linear hygric expansion coefficient α_u at a constant temperature with the varying moisture content is relatively easy. On the contrary, the determination of α_T for porous materials is a little more complicated, since it is technically difficult to keep the absolute moisture content constant when the temperature is changing.

Therefore, in practical measurements [17], we first determine the dependence of the normal strain on moisture at room temperature. The material is moistened either to the full water saturation or to the equilibrium moisture content, and then it is slowly dried with a simultaneous measurement of the length changes. Thus, a relation $\epsilon_u = \epsilon_u(u)$ is obtained over a wide range of moisture and at constant temperature. The function $\epsilon_u(u)$ is represented by point values. Therefore, a regression analysis is necessary to obtain a continuous function. In accordance with Eq. (13), α_u is obtained as the first derivative of $\epsilon_u(u)$. Knowing the function $\alpha_u(u)$, we can continue with the temperature changes. Considering the superposition principle, we first measure the length changes caused by the changing temperature, and simultaneously determine the changes of moisture content. Then, these length changes are recalculated to the zero moisture content using the $\epsilon(u)$ functions which result in a pointwise given function $\epsilon_T = \epsilon_T(T)$ for a constant moisture ($u=0$) as required by Eq. (13). Regression analysis and calculation of the first derivative of $\epsilon_T(T)$ with respect to T lead to the function $\alpha_T = \alpha_T(T)$.

In measuring the high-temperature linear thermal expansion of cement mortar, we employed the experimental device currently developed in our laboratory (see Ref. [18] for details). The device consists of a cylindrical, vertically oriented electric furnace with two bar samples located in the furnace. The first sample is the measured material, the second sample is a reference material with the known dependence of the thermal expansion coefficient on temperature. The length changes of the samples are measured mechanically outside the furnace by thin ceramic rods which pass through the furnace cover and are fixed on the top side of the measured sample. These ceramic rods pass by an undefined temperature field; therefore, their normal strain is not possible to be determined mathematically and a comparative method of determining the normal strain of the rod is used.

In measuring hygric expansion, we have measured the length changes by the Carl Zeiss optical contact comparator with ±1 μm accuracy; the mass changes were determined by the electronic balance Sartorius with ±1 mg accuracy. The basic set of points $l_i(m_i,T_i)$ necessary for the determination of the $\alpha(u)$ function was obtained in this way. The experiments were performed under isothermal conditions, with $T = (25.0 \pm 0.5)$°C.

2.3. Moisture diffusivity

For determination of moisture diffusivity κ, we employed a simple method based on the assumption that κ can be considered as piecewise constant with respect to the moisture density ρ_m (PCK method in what follows). Contrary to the most frequently used methods for κ determination (see Refs. [19–22]), the PCK method is very fast even

for materials with low κ, and in addition, it exhibits a reasonable precision [23]. Therefore, its application for cement mortar is very suitable. The basic idea of the method is as follows.

We assume that the geometry of the experiment is so designed that the problem of moisture transport can be reduced to only one dimension. Thus, we can write in a certain (not very wide) range of moisture the transport equation in the form:

$$\frac{\partial \rho_m}{\partial t} = \kappa \frac{\partial^2 \rho_m}{\partial x^2}, \tag{14}$$

where ρ_m is the moisture density in the sense of the theory of mixtures, i.e., the mass of water per unit volume of the porous body. The initial and boundary conditions can be defined as:

$$\rho_m(x,0) = \rho_2, \tag{15}$$

$$\rho_m(0,t) = \rho_1, \tag{16}$$

$$\rho_m(d,t) = \rho_2, \tag{17}$$

where ρ_2 is the initial moisture density in the specimen, ρ_1 is the maximum moisture density which can be achieved in the material (the bottom surface of the board is in direct contact with water during the moistening process).

The diffusion problem [Eqs. (14)–(17)] can be solved analytically with the result (see Ref. [24]):

$$\rho_m(x,t) = \rho_1 + (\rho_2 - \rho_1)\frac{x}{d} + \frac{2}{\pi} \times \sum_{n=1}^{\infty} \frac{\rho_2 - \rho_1}{n} \sin\left(\frac{n\pi x}{d}\right) \exp\left(-\frac{\kappa n^2 \pi^2 t}{d^2}\right). \tag{18}$$

The total mass of water which penetrated into the sample during the time interval $[0,\tau]$ can be expressed by the relation:

$$m_m(\tau) = S \int_0^d (\rho_m(x,\tau) - \rho_2)\mathrm{d}x. \tag{19}$$

After substituting Eq. (18) into Eq. (19), we get the final transcendent equation for κ:

$$m_m(\tau) - S(\rho_1 - \rho_2)\frac{d}{2} + \frac{2dS}{\pi^2}(\rho_1 - \rho_2) \times \sum_{n=1}^{\infty} \frac{1}{n^2}(1 - \cos(n\pi))\exp\left(-\frac{\kappa n^2 \pi^2 \tau}{d^2}\right) = 0, \tag{20}$$

which can be solved by some of the iterative methods, such as the Newton method. The value of κ determined by the solution of Eq. (20) we award to a characteristic average value of the moisture density in the time interval $[0,\tau]$ [Eq. (21)]:

$$\rho_{m,c} = \frac{m_m(\tau)}{2Sd} + \frac{\rho_2 + \rho_1}{2}. \tag{21}$$

In practical measurements, we perform the experiment with a set of samples with various values of the initial moisture density ρ_2, and determine the corresponding set of values of the moisture diffusivity $\kappa(\rho_{m,c})$. In this way, we obtain a pointwise given $\kappa(\rho_m)$ function, i.e., the dependence of the moisture diffusivity on the moisture density.

2.4. Water vapor permeability

The measuring method for determination of the water vapor permeability δ is, in principle, similar as that for κ (see Ref. [25] for details). The measuring apparatus consists of two airtight glass chambers separated by a plate-type specimen of the measured material. In the first chamber, a state near 100% relative humidity is kept (achieved with the help of a cup of water), while in the second one, there is a state close to 0% relative humidity (set up using some absorption material, such as silica gel). The changes in the mass of water in the cup, Δm_w, and of the silica gel, Δm_a, are measured in dependence on time. In the case that also steady-state measurements are required, the validity of the condition $\Delta m_w = \Delta m_a$ is tested and the experiment continues until this condition is realized. The experiment is carried out under isothermal conditions. Compared to the classical cup method, employed in the most of European and American standards, our experimental setup has the advantage that it is not necessary to keep the constant relative humidity in the whole of the climatizing chamber but only in a relatively small chamber, and that also the flux of water vapor incoming the specimen is measured. As a consequence, even the steady-state measurements in our setup can be significantly faster than in the classical cup method setup.

In the practical determination of δ, we know both incoming and outgoing fluxes of water vapor as functions of time, and assume that δ is constant. As follows from the described experimental setup, also the boundary conditions are of the same type as in the case of κ measuring; the constant initial conditions can be managed easily, for instance, using dry samples. Therefore, we have mathematically the same problem as in Eqs. (14)–(17) and the solution is the same as for κ. The final transcendent equation for δ reads [Eq. (22)]:

$$m_v(\tau) - \frac{M}{RT}\frac{2Sd}{\pi^2}\sum_{n=1}^{\infty}\frac{1}{n^2}(p_s - p_c\cos(n\pi))\cos(n\pi) \times \left(1 - \exp\left(-\frac{\delta RTn^2\pi^2\tau}{Md^2}\right)\right) + \frac{M}{RT}\frac{2S}{\pi}\sum_{n=1}^{\infty}\frac{1}{n} \times \left(1 - \exp\left(-\frac{\delta RTn^2\pi^2\tau}{Md^2}\right)\right)\cos(n\pi)\int_0^d p_0 \times (x')\sin\left(\frac{n\pi x'}{d}\right)\mathrm{d}x' - \frac{M}{RT}(p_s - p_c)\frac{S\delta\tau}{d} = 0, \tag{22}$$

where $m_v(\tau)$ is the mass of water vapor which was absorbed by the dessicant during the time interval τ, R is the universal gas constant, T is the temperature in Kelvin, M the molar mass of water, $p_s(T)$ is the saturated pressure of water vapor at temperature T, p_0 is the initial partial pressure of water vapor in the sample, p_c is the partial pressure of water vapor in the chamber with dessicant (usually $p_c = 0$), d is the thickness of the sample in the direction of water vapor flow.

3. Materials and samples

In our experimental work, we used the samples of cement mortar. The composition of the mixture of cement mortar for one charge was the following: Portland cement ENV 197-1 CEM I 42.5 R (Kraluv Dvur, CZ) 450 g, natural quartz sand with continuous granulometry I, II, III (the total screen residue on 1.6 mm 2%, on 1.0 mm 35%, on 0.50 mm 66%, on 0.16 mm 85%, on 0.08 mm 99.3%) 1350 g, water 225 g.

The mortar was prepared by mixing and compacting using mixing machine and vibrator. The dimensions of the samples were $40\times40\times120$ mm^3 for measurements of linear thermal and hygric expansion and for room temperature measurements of thermal conductivity, $71\times71\times71$ mm^3 for high temperature measurements of thermal conductivity and specific heat; the samples for determining moisture diffusivity and water vapor permeability had cylindrical shape with the diameter of 105 mm and the height of 20 mm. The samples in moulds were left for the first 24 h in a high relative humidity environment under wet cloth. After mould removal, the time remaining to 28 days spent the samples in 20°C water and then they were put in protected external environment (a metal sheet shed) with the relative humidity approximately 65%.

After 28 days, the compressive strength was determined on selected samples (57.4 MPa). The remaining samples were mechanically loaded in several different ways (see below); there also was a group of samples which was left without any load, for the sake of comparison.

4. Experimental results

4.1. Thermal conductivity

The measurements of the influence of moisture on the thermal conductivity of cement mortar were performed in isothermal conditions, $T=(25.0\pm0.5)$°C. Before the measurements, different levels of compressive stress were applied on five groups of specimens: (1) zero load (NL in what follows); (2) 90% of compressive strength in the direction of heat flux (i.e., specimens in the flat position, load applied at the 4×12 cm^2 face — F90); (3) first 70% and then 90% of compressive strength in the direction of heat flux (F70+F90); (4) first 57% and then 79% of compressive strength in the direction perpendicular to the heat flux (i.e., the specimens in the standing position, load applied at the 4×4 cm^2 face — S57+S79); (5) 57% of compressive strength perpendicular to the heat flux.

The measured results show (see Fig. 1) that for all samples analyzed, two regions of different $\lambda(u)$ behavior can be distinguished. In the area of lower moistures, typically $u<6.5\%$ kg/kg, the $\lambda(u)$ relation can be approximated by a linear function, increasing with u. This region is roughly equal to the hygroscopic moisture range; the maximum hygroscopic moisture content was determined as

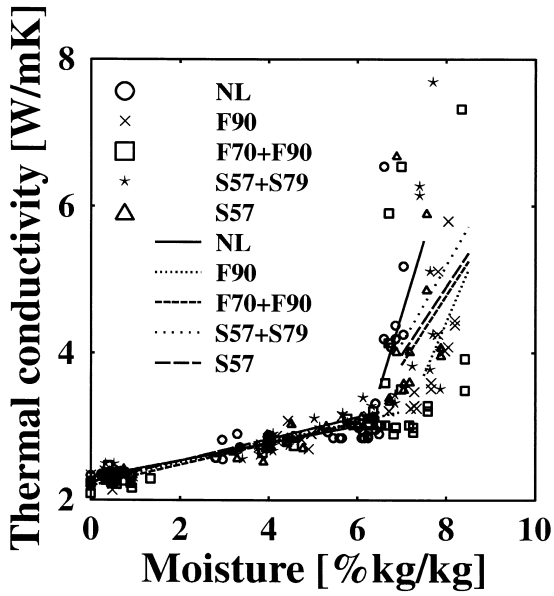

Fig. 1. Thermal conductivity vs. moisture relation of cement mortar at $T=25$°C, depending on the compressive stress applied.

$\sim6\%$ kg/kg. On the other hand, for higher values of the moisture content, i.e., in the overhygroscopic region, the experimental data were very split in all cases. We could not identify any reasonable functional relationship between the thermal conductivity and moisture content in this region. The only feature of the $\lambda(u)$ function was that it increases very fast with u. Nevertheless, we also have performed linear regression in order to get at least a rough view, for the sake of comparison of the influence of various levels of mechanical loading.

In the area of lower moisture content ($u<6.5\%$), we did not find any substantial difference due to the mechanical load applied. The linearly approximated data did not differ by more than 5–8% from each other, which is within the scatter band of the experimental hot wire method.

For higher moisture content, the comparison was rather difficult because the data were very split. However, certain features could be identified in this case anyway. The first was that for unloaded samples (NL), the maximum moisture content u_{max} was $\sim7\%$ but for S57 and S57+S79 samples, we found $u_{max}\sim8\%$, and for F90 and F70+F90 was $u_{max}\sim8.5\%$. This is a clear evidence of the effect of mechanical load which apparently has led to an increase of the pore volume, crack appearance, and partial destruction of the porous structure. Even our rough linear approximation shows that the $\lambda(u)$ functions corresponding to the samples exposed to higher load are shifted to the direction of higher moistures.

Another feature was that even for the highest values of moisture content ($u\sim8$–8.5%), some experimental data for λ lied very close to the extrapolations of the $\lambda(u)$ lines obtained for the lower moisture region, but on the other hand, some of the λ values were two to three times higher.

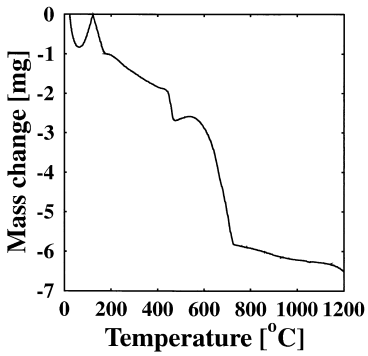

Fig. 2. Dependence of density of cement mortar on temperature.

This seems to be an evidence that the porous structure was damaged only locally, and our measured values of λ depended very strongly on the exact position of the hot wire probe on the particular specimen.

For the high temperature measurements, we used two types of samples, the first group was not exposed to any load (NL), the second one was exposed to the mechanical load 90% of compressive strength perpendicular to the direction of heat flux (ML).

Before measurements of thermal conductivity, we had to perform the measurements of density and specific heat in dependence on temperature. The results of thermogravimetric measurements are in Fig. 2, specific heat vs. temperature relation is given in Fig. 3.

The results of high temperature measurements of thermal conductivity are shown in Fig. 4. Apparently, an increase of thermal conductivity ranging from 5% to 30% was observed in the whole temperature region studied.

4.2. Linear thermal expansion coefficient

The measurements of linear thermal expansion were performed on 12 samples which were approximately 8 months old. One third of the samples was not exposed to any load (we will denote it NL in what follows), the second third was mechanically loaded to 69.5% of compressive strength flat (i.e., the load in the direction

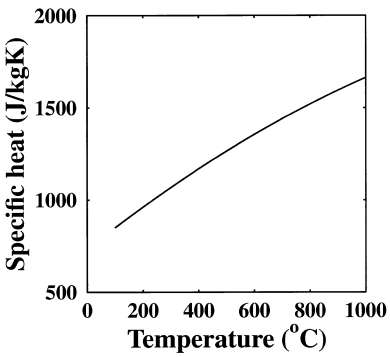

Fig. 3. Dependence of specific heat of cement mortar on temperature.

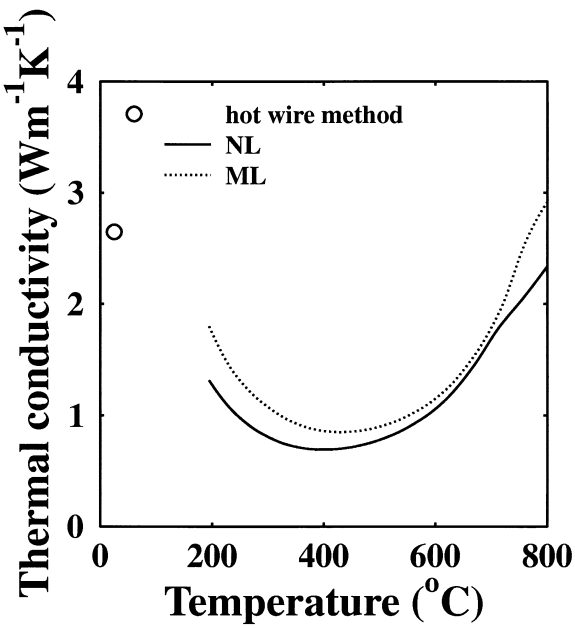

Fig. 4. Thermal conductivity vs. temperature relation of cement mortar for dry samples.

parallel to the 40×40 mm^2 face, in the center of the 40×120 mm^2 face — it will be denoted as F69), the final third to 57.3% of compressive strength standing (i.e., the load in the direction parallel to the 40×120 mm^2 face, in the center of the 40×40 mm^2 face — it will be denoted as S57).

Fig. 5 shows the dependence of the linear thermal coefficient α_T on temperature in the range of 20–1000°C for the three mentioned cases.

Generally, the character of all three curves in Fig. 5 remains similar, the $\alpha(T)$ functions increase up to 500°C

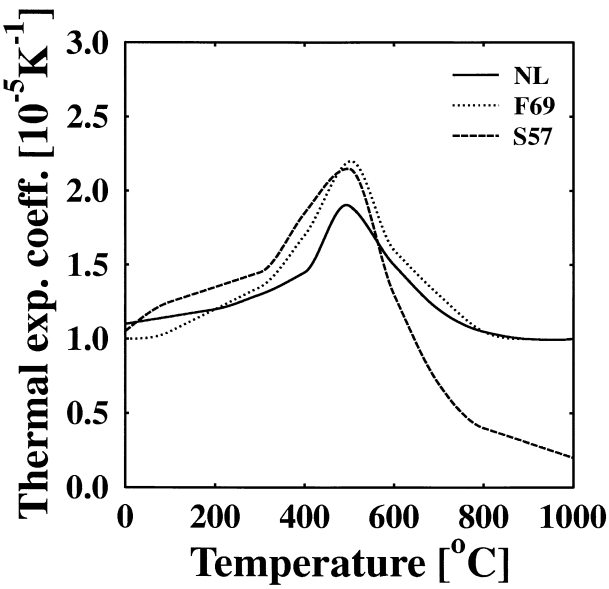

Fig. 5. Linear thermal expansion coefficient of cement mortar.

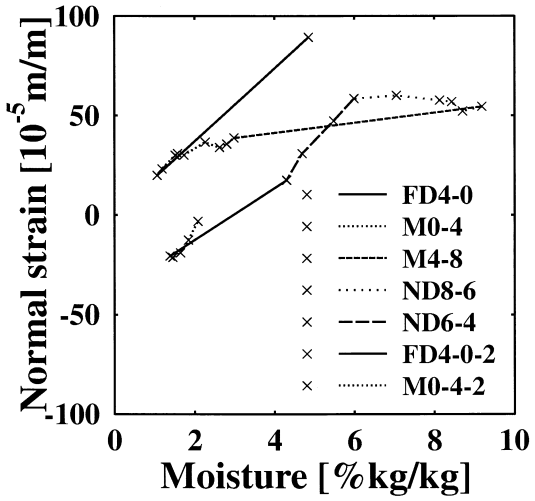

Fig. 6. Normal strain as function of the way of moistening and drying for S57 sample.

and then decrease. This decrease is for the case of NL and F69 samples practically the same as the foregoing increase, and for 1000°C, the values of α are practically the same as for 20°C, but for S57 samples, the $\alpha(T)$ function decreases much faster. The interesting moment is that the remarkable differences between $\alpha(T)$ functions of F69 and S57 appear in the higher temperature region only, $T>500$°C. Practically, it means that combination of damage due to the mechanical and thermal load was effective for the standing position of the sample and higher temperatures only; otherwise, the thermal damage prevailed.

4.3. Linear hygric expansion coefficient

The measurements of moisture expansion were performed on 21 samples which were approximately 8 months old. One third of the samples was not exposed to any load (we will denote it NL in what follows), the second third was mechanically loaded to 69.5% of compressive strength flat (i.e., the load in the direction parallel to the 40×40 mm^2 face, in the center of the 40×120 mm^2 face — it will be denoted as F69), the final third to 57.3% of compressive strength standing (i.e., the load in the direction parallel to the 40×120 mm^2 face, in the center of the 40×40 mm^2 face — it will be denoted as S57). As the continuous measurements have shown relatively small differences between the unloaded and loaded samples, another load was put to the samples previously loaded; for the flat orientation, it was to 89.6% of compressive strength (F89), for the standing orientation, to 79.3% (S79).

Table 1
Linear hygric expansion coefficient of cement mortar in 10^{-5} (% kg/kg)$^{-1}$ for various regimes of moistening and drying and various mechanical loads

Sample/region	FD4-0	M0-4	M4-8	ND8-6	ND6-4
NL	14.7	24.6	1.4	2.4	18.8
S57	19.0	25.1	2.80	2.5	27.0
F69	15.2	24.8	3.4	2.9	16.0
S79	21.4	23.1	23.1	2.5	22.5
F89	16.6	25.4	25.4	2.6	21.2

Table 2
Hygric parameters of cement mortar

Sample	κ (10^{-9}m^2/s)	δ (10^{-12} s)
NL	3.1	3.43
T38	4.7	2.86
T79	4.2	2.98
S90	49.0	3.87

Fig. 6 shows an example of the measured normal strains where only one characteristic sample of the seven, which were measured, is shown for the sake of clarity. Apparently, several regions with abrupt changes of the first derivative with respect to moisture (i.e., of the moisture expansion coefficient) can be identified, namely, the forced drying from $u=4\%$ to $u=0$ (FD4-0 in what follows), the moistening on the air with 40% relative humidity (M0-4), the moistening in water (M4-8), natural drying from the full water saturation (ND8-6), and natural drying in the hygroscopic region (ND6-4). Table 1 shows the average values of α_u of samples mechanically loaded as defined before and in the mentioned regions of moistening and drying.

The results can be summarized as follows. The mechanical load before the measurements has a relatively little influence on the moisture expansion coefficient α_u. In general, for higher load, higher values of α_u were observed; for the standing orientation of the sample, higher α_u values compared to the flat orientation were measured.

4.4. Moisture diffusivity and water vapor permeability

The experimental results of measurements of hygric parameters are summarized in Table 2. Apparently, both δ and κ were almost unaffected by the mechanical load in a relatively wide range; for the loads up to approximately 80% of compressive strength, the differences were within the scatter band of experimental measurements. First, the load of 90% of compressive strength has led to significant changes in the hygric parameters, more pronounced was this effect for liquid moisture diffusivity which increased by one order of magnitude compared to the lower values of load.

5. Discussion

In order to analyze the reasons for the remarkable changes in thermal and hygric parameters induced by mechanical load, we used scanning electron microscopy (SEM), mercury porosimetry (MP) and differential thermal analysis (DTA).

Scanning electron microscope Jeol JXA-733 was employed to study the structural changes in the surface region of the samples induced by mechanical load. Typical results are shown in Figs. 7 and 8. Fig. 7 represents the sample

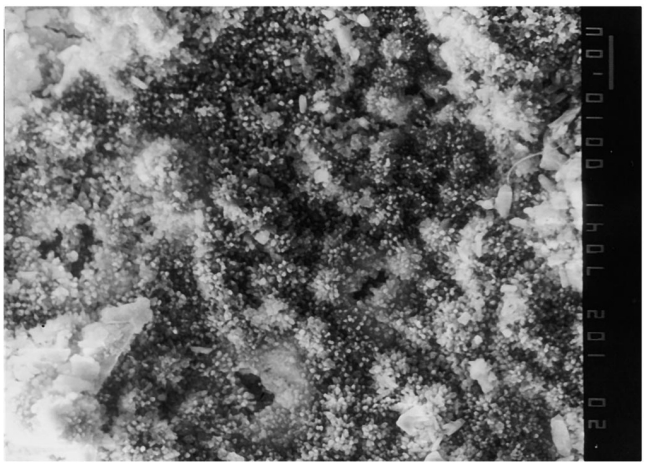

Fig. 7. SEM image of an unloaded sample; 9 mm on the picture represents 10 μm on the sample.

without any load in the 1000 enlargement. Apparently, no visible cracks appear on the picture. Fig. 8 shows the sample loaded in the standing position to 90% of compressive strength (S90) in two same 1000 enlargements. The typical crack shown in this figure has the width of approximately 1–2 μm.

Porosimetric measurements were performed using the mercury porosimeter AutoPore 200 Micromeritics on two types of specimens. While the first specimen was not exposed to any load (NL according to our previous notation), the second was exposed to mechanical load of 90% of compressive strength (S90).

The results are shown in Table 3 and Fig. 9. Table 3 presents a summary of global characteristics of the particular specimens, V_p is the total intrusion volume, A_p the total pore area, r_v the median pore radius by volume, ρ the volume mass of the material. Apparently, the application of mechanical load has led to some changes in global

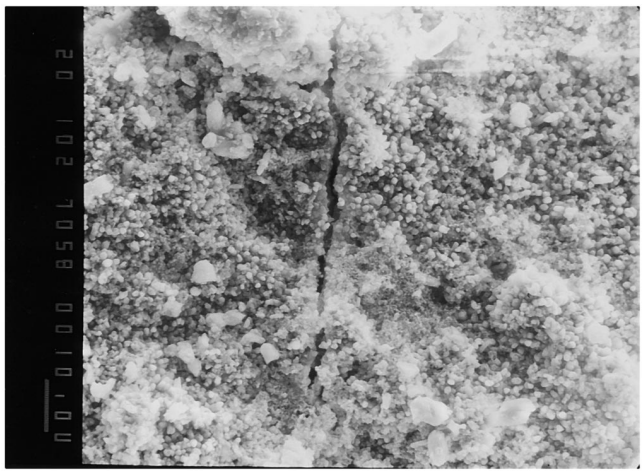

Fig. 8. SEM image of a sample loaded to 90% of compressive strength (S90); 9 mm on the picture represents 10 μm on the sample.

Table 3
Global characteristics of the porous space

Specimen	V_p (cm^3/g)	A_p (m^2/g)	r_v (μm)	ρ (kg/m^3)
NL	0.065	15.89	0.033	2250
S79	0.072	11.77	0.043	2180

parameters; for instance, V_p increased by 10%, r_v increased by 30%, and A_p decreased by 26% compared to the reference specimen NL, which is an evidence of increase of amount of bigger pores.

Fig. 9 shows a comparison of differential distribution functions of the pore volume by pore radius for the studied specimens. We can see that mechanical load of 90% of compressive strength has led to certain increase of pore volume in the region 0.3–2 μm compared to the reference specimen NL which complements our findings from the global characteristics. This is in a qualitative agreement with the results of SEM measurements which revealed for mechanically loaded specimens an appearance of not very numerous cracks 1–2 μm in width. Therefore, we believe that crack appearance due to the mechanical load was the main reason for the observed changes in the porous structure.

Fig. 10 shows the results of DTA measurements which are apparently very regular. We can identify all common peaks, namely H_2O, CSH, CAH, $Ca(OH)_2$, $SiO_2(\beta \rightarrow \alpha)$, $CaCO_3$, respectively.

The appearance of 1–2 μm wide cracks, which have been found by SEM and MP, should affect the hygric parameters in a remarkable extent, and it is quite logical that their influence on moisture diffusivity, which is usually very low in concrete and cement mortar, was very significant and more pronounced than on the parameters of much

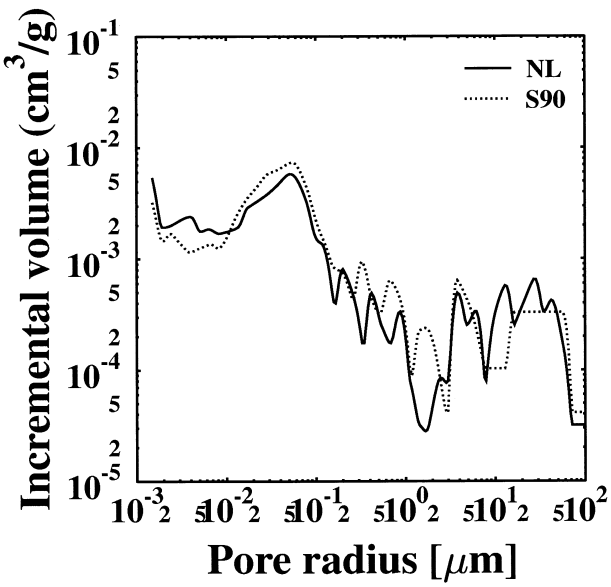

Fig. 9. Differential distribution functions of the pore volume of the analyzed specimens of cement mortar.

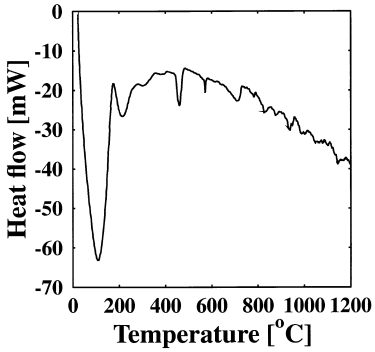

Fig. 10. DTA curve of cement mortar.

faster vapor transport. In this respect, it should be noted that the PCK method for determination of liquid moisture diffusivity is very simple and in some cases, it can lead to significant errors compared to the more established methods. An analysis of the properties of this method was given in Ref. [23]. It was shown that the PCK method in its current form can give reasonable results for the range of higher moistures only, typically 50% of the saturation moisture content and more, and for lower moistures, it is not suitable. Also, it was demonstrated that for well homogeneous materials such as extruded porcelain mixture, the deviations of results obtained by the Boltzmann–Matano method and double integration method were relatively low, ±10% in maximum which is a reasonable precision. However, for less homogeneous materials as cementitious fiber composites, the deviations were significantly higher, up to 50%. As cement mortar concerning the homogeneity lies somewhere between these two types of materials, it can be anticipated that a characteristic deviation from results obtained by more established methods may lie between 10% and 50%. Therefore, we can confirm that the measured differences in κ for mechanical load up to 90% were not significant from the point of view of measuring accuracy, but the one order of magnitude difference observed for the S90 specimens was apparently significant even with the application of this simple method.

The higher values of thermal conductivity in the overhygroscopic region (6–8 W/mK as we have found in some measurements) probably cannot result from solely heat conduction (for water, we have λ=0.63 W/mK, and for the air λ=0.026 W/mK), but a combination of conduction and convection effects takes place here, particularly in the parts of the sample where the porous structure is damaged. The appearance of wide cracks supports this hypothesis.

The increase of thermal conductivity induced by the mechanical load in the high temperature region might possibly also be awarded to the convective effects which were more pronounced here due to both temperature and pressure gradients. A simple analysis of moisture transport effects shows that for a high temperature measurement taking about 30 min, the characteristic length of moisture transport is ~1.5 mm for NL specimens and ~4 mm for S90 specimens. This is probably too low to affect the heat transfer in a significant way. However, this estimate follows from an assumption of pure diffusion moisture transport where the moisture gradient is the only driving force. In reality, the gradient of pore pressure in the specimen induced by water evaporation at higher temperatures can probably be considered as a much stronger driving mechanism affecting water transport and consequently also heat transport. Unfortunately, we cannot estimate the magnitude of this effect in a serious way because we did not measure the capillary pressures in our experiment. This kind of measurement in the high temperature range is an extremely difficult task.

The remarkable differences between α_u values (both at moistening and drying) in the hygroscopic and overhygroscopic regions can be explained by the mode of water penetration into the porous body in these two regimes. While in the hygroscopic region the most important way of the incorporation of the molecules of water into the porous structure is their absorption on the pore walls, where first monomolecular and later polymolecular layers are formed (and the surface phase of water prevails over the volume phase as a consequence), in the overhygroscopic region, the water penetrates into the porous structure as a volume phase mostly and fills the inside of the pores as the pore walls are already covered by the surface phase of water.

The irreversible changes in the length of the sample following, on one hand, their saturation to the maximum water content and, on the other their, forced drying in the hot air dryer are most probably consequences of the late hydration of cement and ablation of microparticles by water. Also, the effect of microcracking induced by differences in moisture concentration between the specimen core and its surface during the drying process might play a significant role. To that point, the forced drying process FD4-0 can be considered as the most dangerous. Assuming the moisture expansion coefficient $\sim 20\times10^{-5}$ $(\%\mathrm{kg/kg})^{-1}$ and the maximum difference in moisture concentrations in the specimen ~4% kg/kg, we obtain, by a simple elastic analysis, the maximum estimated hygric stresses of about 50 MPa which is high enough to microcracks appearance.

6. Conclusions

The thermal conductivity vs. moisture relation $\lambda(u)$ in isothermal room temperature conditions was found to be unaffected by the mechanical load up to 90% of compressive strength only in the region of hygroscopic moisture content. In the overhygroscopic region, the $\lambda(u)$ functions were shifted to the direction of higher moistures and the experimental data exhibited a much wider scatter band than in the hygroscopic region. In the higher temperature range, $T\in$[200°C, 800°C], the thermal conductivity of samples exposed to 90% of compressive strength load was found to be 5–30% higher compared to the unloaded samples.

The linear thermal expansion coefficients of samples of cement mortar both mechanically unloaded and loaded in two different ways were determined in wide temperature range of 20–1000°C. The low temperature data correspond well to the usual values of α_T for concrete. In the high temperature region, the $\alpha_T(T)$ functions have a maximum at approximately 500°C. The position of the $40 \times 40 \times 120$ mm^3 samples during mechanical loading was found to have a remarkable influence on the values of α_T in the higher temperature region only, for $T > 500$°C. Generally, the effect of thermal load prevailed over that of mechanical load in the studied situation.

The mechanical load up to 90% of the compressive strength was found to have a relatively low effect on the hygric expansion coefficient of cement mortar. On the other hand, the way of moistening and drying has appeared as a very remarkable effect which can result in variations as high as one order of magnitude in the hygric expansion coefficient. These variations are mainly due to the way of incorporation of water molecules into the porous structure (or water removal from it) and due to the late hydration processes caused by either full water saturation or by heating in the dryer.

In measuring the influence of mechanical load on the liquid moisture diffusivity κ and water vapor permeability δ, it has been observed that up to 80% of compressive strength, no remarkable changes appeared; they became significant first at the level of 90% of compressive strength.

From the practical point of view, the results look very promising because there are not so many concrete structures which are loaded to more than 90% of compressive strength. However, it should be noted that only first experimental results were presented in this paper which were concentrated to an immediate load application only, and the measurements were performed after load removal. Further experimental work is necessary to analyze, for instance, the influence of long-term loads, with the measurements of thermal and hygric parameters being performed during the load exposure.

Acknowledgments

This research has been supported by the Grant Agency of the Czech Republic, under grant nos. 103/00/0021 and 103/97/K003.

References

[1] R. Philleo, Some physical properties of concrete at high temperatures, J Am Concr Inst 29/54 (1958) 857–864.
[2] T. Harada, J. Takeda, S. Yamane, F. Furumura, Strength, elasticity and thermal properties of concrete subjected to elevated temperatures, International Seminar on Concrete for Nuclear Reactors 1, American Concrete Institute, Detroit, 1972, pp. 377–406, ACI Special Publication No. 34, Paper SP34-21.
[3] U. Schneider, Behaviour of concrete at high temperatures, Deutscher Ausschuss fuer Stahlbeton, Heft 337, W. Ernst and Sohn, Berlin, 1982, pp. 1–122.
[4] A.N. Komarovskii, Design of Nuclear Plants, 2nd edn., Atomizdat, Moscow, 1965, pp. 115–134 (in Russian).
[5] T.Z. Harmathy, Thermal properties of concrete at elevated temperatures, ASTM J Mater 5 (1970) 47–74.
[6] T.Z. Harmathy, L.W. Allen, Thermal properties of selected masonry unit concretes, J Am Concr Inst 70 (1973) 132–142.
[7] G. Hildenbrand, M. Peeks, A. Skokan, M. Reimann, Investigations in Germany of the barrier effect of reactor concrete against propagating molten Corium in the case of a hypothetical core meltdown accident of an LWR, ENS/ANS International Meeting on Nuclear Power Reactor Safety, Vol. 1, Brussels, 1978, pp. 16–19.
[8] Z.P. Bažant, M.F. Kaplan, Concrete at High Temperatures: Material Properties and Mathematical Models, Longman, Harlow, 1996.
[9] Z.P. Bažant, L.J. Najjar, Non-linear water diffusion in non-saturated concrete, Materials and Structures, Vol. 5, RILEM, Paris, 1972, pp. 3–20.
[10] T.C. Powers, T.L. Brownyard, Studies of the physical properties of hardened cement paste, Research Department Bulletin, Vol. 22, Portland Cement Association, Chicago, 1948.
[11] A.S. El-Dieb, R.D. Hooton, Water permeability measurement of high performance concrete using a high-pressure triaxial cell, Cem Concr Res 25 (1995) 1199–1208.
[12] P. Halamickova, R.J. Detwiler, D.P. Bentz, E.J. Garboczi, Water permeability and chloride diffusion in Portland cement mortars: relationship to sand content and critical pore diameter, Cem Concr Res 25 (9) (1995) 790–802.
[13] Z.P. Bažant, W. Thonguthai, Pore pressure and drying of concrete at high temperature, J Eng Mech Div ASCE 104 (1978) 1059–1079.
[14] P. Bažant, S. Sener, J.K. Kim, Effect of cracking on drying permeability and diffusivity of concrete, ACI Mater J 84 (1987) 351–357.
[15] R. Černý, J. Toman, Solution of inverse problems of heat conduction in building materials, in: R.W. Lewis, J.T. Cross (Eds.), Proceedings of Numerical Methods in Thermal Problems 10, Pineridge Press, Swansea, 1997, pp. 811–820.
[16] J. Toman, R. Černý, High-temperature measurement of the specific heat of building materials, High Temp–High Pressures 25 (1993) 643–647.
[17] J. Toman, R. Černý, Coupled thermal and moisture expansion of porous materials, Int J Thermophys 17 (1996) 271–277.
[18] R. Černý, J. Toman, T. Klečka, Thermal expansion of concrete at high temperatures, in: T.J. vor (Ed.), Proceedings of Non-Destructive Testing and Experimental Stress Analysis of Concrete Structures, Expertcentrum, Bratislava, 1998, pp. 146–151.
[19] C. Matano, On the relation between the diffusion coefficient and concentration of solid metals, Jpn J Phys 8 (1933) 109–115.
[20] I. Kašpar, Moisture Transport in Building Materials, DrSc Thesis, CTU, Prague, 1984 (in Czech).
[21] P. Häupl, H. Stopp, H. Ein, Beitrag zum Feuchtigkeitstransport in Bauwerksteilen, Schriftenr Sektion Archit TU Dresden 16 (1980) 93–103.
[22] J. Drchalová, R. Černý, Non-steady-state methods for determining the moisture diffusivity of porous materials, Int Comm Heat Mass Trans 25 (1998) 109–116.
[23] J. Drchalová, R. Černý, J. Havrda, Analysis of some aspects in determining the anisotropy of moisture transfer in building materials, Proceedings of New Requirements for Materials and Structures, CTU Press, Prague, 1998, pp. 194–199.
[24] H.S. Carslaw, J.C. Jaeger, Conduction of Heat in Solids, 2nd edn., Clarendon Press, Oxford, 1960.
[25] R. Černý, Š. Hošková, J. Toman, A transient method for measuring the water vapor diffusion in porous building materials, in: V.P. de Freitas, V. Abrantes (Eds.), Proceedings of International Symposium on Moisture Problems in Building Walls, University of Porto, Porto, 1995, pp. 137–146.